# Functional role of catalytic triad and oxyanion hole-forming residues on enzyme activity of *Escherichia coli* thioesterase I/protease I/ phospholipase $L_1$

Li-Chiun LEE*, Ya-Lin LEE†[1], Ruey-Jyh LEU‡ and Jei-Fu SHAW*‡§[1]

*Institute of Bioscience and Biotechnology, National Taiwan Ocean University, Keelung, 20224, Taiwan, †Department of Nutrition and Food Sciences, Fu-Jen Catholic University, Taipei County, 24205, Taiwan, ‡Institute of Botany, Academia Sinica, Nankang, Taipei, 11529, Taiwan, and §Department of Food Science and Biotechnology, National Chung Hsing University, Taichung, 40227, Taiwan

*Escherichia coli* TAP (thioesterase I, EC 3.1.2.2) is a multifunctional enzyme with thioesterase, esterase, arylesterase, protease and lysophospholipase activities. Previous crystal structural analyses identified its essential amino acid residues as those that form a catalytic triad ($Ser^{10}$-$Asp^{154}$-$His^{157}$) and those involved in forming an oxyanion hole ($Ser^{10}$-$Gly^{44}$-$Asn^{73}$). To gain an insight into the biochemical roles of each residue, site-directed mutagenesis was employed to mutate these residues to alanine, and enzyme kinetic studies were conducted using esterase, thioesterase and amino-acid-derived substrates. Of the residues, $His^{157}$ is the most important, as it plays a vital role in the catalytic triad, and may also play a role in stabilizing oxyanion conformation. $Ser^{10}$ also plays a very important role, although the small residual activity of the S10A variant suggests that a water molecule may act as a poor substitute. The water molecule could possibly be endowed with the nucleophilic-attacking character by $His^{157}$ hydrogen-bonding. $Asp^{154}$ is not as essential compared with the other two residues in the triad. It is close to the entrance of the substrate tunnel, therefore it predominantly affects substrate accessibility. $Gly^{44}$ plays a role in stabilizing the oxyanion intermediate and additionally in acyl-enzyme-intermediate transformation. N73A had the highest residual enzyme activity among all the mutants, which indicates that $Asn^{73}$ is not as essential as the other mutated residues. The role of $Asn^{73}$ is proposed to be involved in a $loop_{75-80}$ switch-move motion, which is essential for the accommodation of substrates with longer acyl-chain lengths.

Key words: catalytic triad, enzyme kinetics, esterase, oxyanion hole, site-directed mutagenesis, thioesterase I (TAP).

## INTRODUCTION

Lipases and esterases are widely distributed in Nature and they also have multifunctional activities in industrial applications such as the hydrolysis of lipids, the synthesis of esters, thioesters and amides, and the kinetic resolution of racemic mixtures [1,2]. Through protein database mining, Upton and Buckley [3] generalized a lipolytic family with diverse substrate specificity that contain a GDSLS motif (with the active-centre serine located near the N-terminus) and five consensus blocks with homologous amino-acid-sequence arrangement (shown in Figure 1). Previously, a subgroup of the GDSL family, derived from the aforementioned lipolytic family, was classified further as SGNH-hydrolases due to the presence of four strictly conserved residues, Ser-Gly-Asn-His, in the four conserved blocks I, II, III, and V respectively (Figure 1) [4,5]. We have also reviewed a number of enzymes in the GDSL family, which show a broad range of substrate specificies [6].

Our group was the first to report on the arylesterase (EC 3.1.1.2) from *Vibrio mimicus* [7,8] and the multiple functions of thioesterase I/protease I from *Escherichia coli* [9,10]. Both proteins belong to the GDSLS family and show a 51.7 % sequence similarity [7]. TAP (thioesterase I, EC 3.1.2.2) consists of 182 amino acid residues, with a molecular mass of 20.5 kDa [11]. It specifically catalyses the deacylation of fatty acyl-CoA thioesters from fatty acyl-acyl carrier proteins, especially those with long acyl groups ($C_{12}$–$C_{18}$). Since several different names – including thioesterase I, protease I, and lysophospholipase $L_1$ – have been used in the literature for the versatile activities of the protein, the gene product was designated TAP, on the basis of the chronological order of the discovery of the gene (*TesA*/*ApeA*/*PldC*) [11–18]. In previous studies, the secondary structure was solved using NMR [19,20] and X-ray crystallography [21,22]. These two methods illustrated slight structural differences that are shown in Figure 1. NMR analyses indicated that TAP consists of a four-strand parallel $\beta$-sheet and seven $\alpha$-helices (Figure 1), with a folding topology of an $\alpha/\beta/\alpha$ type. TAP forms a tetramer at pH values above 6.5, while existing as a monomer at lower pH values [19]. Both monomeric and tetrameric forms were shown to be catalytically active at a pH greater than 5.0 [10]. The crystallographic structure of TAP (PDB code 1IVN) with 1.95 Å resolution (1 Å = 0.1 nm) has further identified $Ser^{10}$, $Asp^{154}$ and $His^{157}$ as the residues that form the catalytic triad [21], and another two conserved residues $Gly^{44}$ and $Asn^{73}$ (in SGNH) [22]. The secondary structure deposited into the PDB consists of five $\beta$-strands and 11 helices, made up of seven $\alpha$-helices and four $3_{10}$-helices (Figure 1). The crystal co-ordinates were plotted using the ViewerLite (version 5.0, Academic Version; Accelrys Inc.) program, and show a similar secondary structure (Figure 2), with only minor differences compared with the structure of the reported crystal protein (presented in Figure 1).

In the present study, several residues related to the catalytic activity of TAP were mutated to alanine by site-directed mutagenesis. The enzymatic activities of the mutants were analysed

Abbreviations used: $C_{12}$-CoA, lauroyl-CoA; DEP, diethyl *p*-nitrophenyl phosphate; IPTG, isopropyl $\beta$-D-thiogalactoside; LB, Luria–Bertani; L-NBTNPE, *N*-carbobenzoxy-L-tyrosine *p*-nitrophenyl ester; Ni-NTA, $Ni^{2+}$-nitrilotriacetate; NPB, *p*-nitrophenyl butyrate; TAP, thioesterase I; TAP-OCA, native TAP soaked with octanoic acid.

[1] Correspondence may be addressed to either J.-F. S. (email presid@dragon.nchu.edu.tw) or Y.-L. L. (email nutr2032@mails.fju.edu.tw).

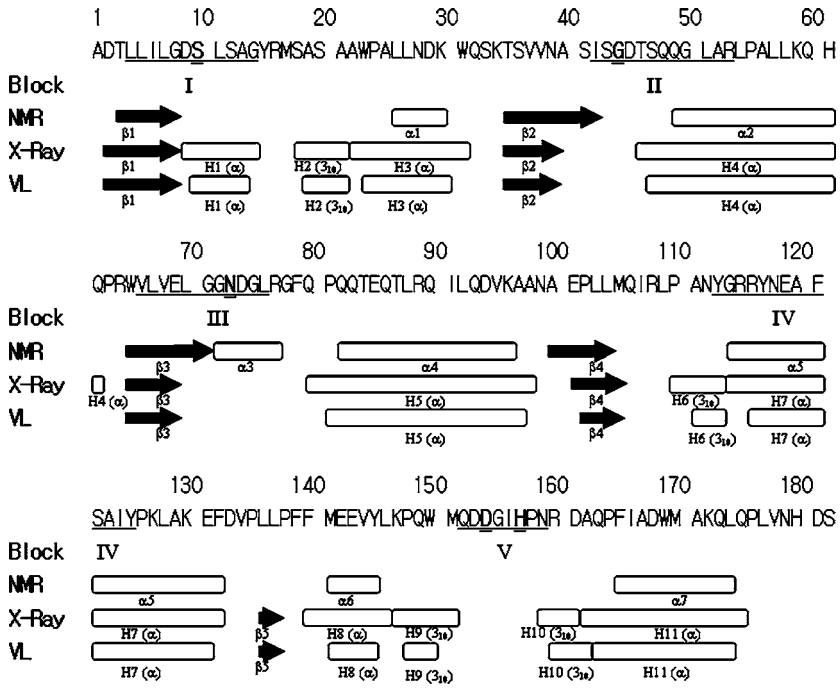


**Figure 1 Secondary structures of TAP solved by NMR [19] and crystallography [22]**

Black arrows represent $\beta$-strands and oblongs represent helices including $\alpha$-helix and $3_{10}$-helix. There are five sequence-conserved blocks (I–V) and the corresponding residues located in TAP are underlined. Ser[10], Gly[44], Asn[73], Asp[154] and His[157] are marked in bold and are double-underlined. The structure solved by NMR is composed of four $\beta$-strands to form a four-stranded parallel $\beta$-sheet and seven $\alpha$-helices. The structure solved by crystallography consists of a five-stranded parallel $\beta$-sheet, four $3_{10}$ helices and seven $\alpha$-helices (PDB code 1IVN). The co-ordinates of the crystal structure shown in the VL line and were plotted using the ViewerLite (version 5.0) program. This shows only minor differences compared with the crystal structure, which are the result of the slight differences in the secondary-structure definition.

using three different substrates: NPB (*p*-nitrophenyl butyrate), which represents a simple ester, for use in the esterase activity assay; $C_{12}$-CoA (lauroyl-CoA), which represents a medium acyl-chain-length thioester, for use in the thioesterase activity assay, and; L-NBTNPE (*N*-carbobenzoxy-L-tyrosine *p*-nitrophenyl ester), which represents an aromatic amino-acid-derived ester substrate. The kinetic parameters of the mutants provide direct information on substrate binding affinity ($K_m$) and catalytic efficiency ($k_{cat}/K_m$). Combined with the protein structures revealed by NMR and crystallography, these results have provided insights into the structure and essential residues of one member of the GDSL- and SGNH-hydrolase families.

## EXPERIMENTAL

### Materials

Oligonucleotide primers were made by DNAFax Co. (Taipei, Taiwan, Republic of China). Taq DNA polymerase and DNA sequencing kit were obtained from HT Biotechnology Ltd (Cambridge, U.K.) and US Biochemicals (Cleveland, OH, U.S.A.) respectively. IPTG (isopropyl $\beta$-D-thiogalactoside) was obtained from Boehringer Mannheim Biochemicals. Substrates of NPB, $C_{12}$-CoA and L-NBTNPE were purchased from Sigma. Restriction enzymes were purchased from Promega Biosciences. Ni-NTA ($Ni^{2+}$-nitrilotriacetate) resin ($His_6$-binding resin) was purchased from Novagene. Protein molecular-mass markers were purchased from Novex.

### Construction of the wild-type *TAP* gene in *E. coli*

The recombinant *TAP* gene with a $His_6$-tag coding sequence fused to the 3′-end, was designated as ‘wild-type’ and was synthesized from a plasmid containing the *tesA* gene [11] by PCR [7]. The 5′-end of the forward primer (5′-GAAGGAGATATACATATGGCGGACACGTTA-3′) and 3′-end of the reverse primer (5′-GTGGTGGTGCTCGAGTGAGTCATGATTTAC-3′) were designed to introduce sites for digestion by the restriction enzymes NdeI and XhoI respectively (the restriction enzyme sites are underlined in the primers). After restriction enzyme digestion, the PCR products were ligated into the pET 20b(+) vector (Novagene), which had been linearized using NdeI and XhoI. To obtain the constructed plasmid, it was transformed into *E. coli* DH5$\alpha$ cells (Promega Biosciences). The sequence of the recombinant gene was confirmed by full-length DNA sequencing. The verified plasmid was transformed into *E. coli* BL21(DE3) cells (Novagene) for target gene overexpression.

### Site-directed mutagenesis

The catalytic-triad residues, Ser[10]-Asp[154]-His[157], as well as the oxyanion-related residues, Gly[44] and Asn[73], were mutated to alanine. The mutagenesis was carried out by overlap-extension PCR, which consisted of two stages [8]. The first PCR stage simultaneously generates two PCR fragments: the first used a 5′-forward primer and a 3′-reverse primer that contains the mutation, the other used a 5′-forward primer that contains the mutation and a 3′-reverse primer. The second stage was carried out using the wild-type gene as the template, to which both PCR products from the first stage could anneal. The extension was performed between the 5′-end forward and 3′-end reverse primers. The PCR primers designed for site-directed mutagenesis are summarized in Table 1 (only the sense sequences are listed, and the corresponding mutation primers are the antisense sequences). A plasmid preparation kit (Qiagen) was used to purify the PCR products by

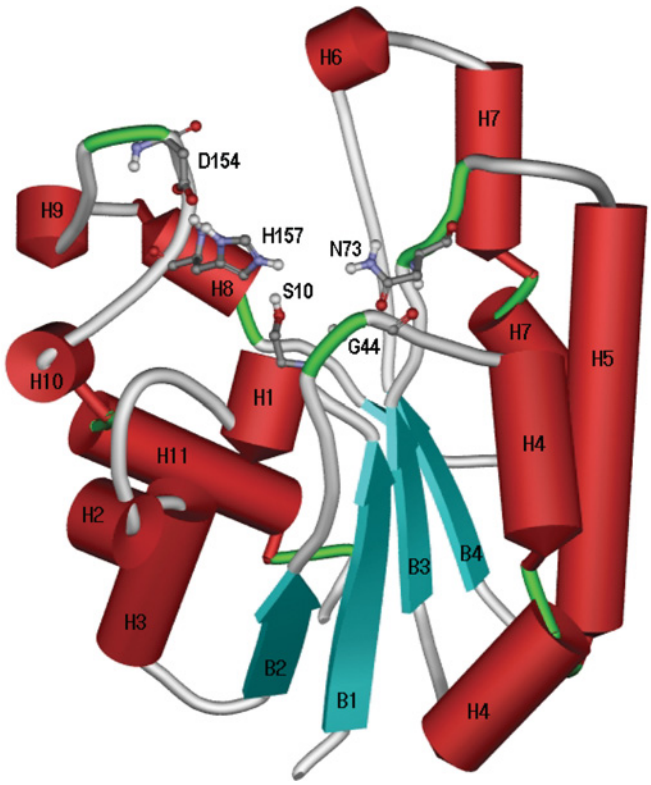


**Figure 2 Overall structure of TAP**

The three-dimensional structure of TAP was solved by crystallography (PDB code 1IVN), and prepared using the ViewerLite (version 5.0) program, showing 11 helices and a five-stranded parallel $\beta$-sheet. The indicated residues are the catalytic triad, $Ser^{10}$-$Asp^{154}$-$His^{157}$, and the stabilizing oxyanion residues, $Gly^{44}$ and $Asn^{73}$. H represents helices, including $\alpha$-helices and $3_{10}$-helices. B represents $\beta$-strands, and B5 located behind B4 is not labelled. $Ser^{10}$ (conserved in block I, as shown in Figure 1) serves as a nucleophile, and its amide proton can be devoted to hydrogen-bonding with oxyanion, a tetrahedral-carbon-covalent acyl-enzyme intermediate (shown in Figure 5). The $Gly^{44}$ residue (conserved in block II, as shown in Figure 1), whose amide proton is devoted to hydrogen-bonding with oxyanion, is located in a loop region. $Asp^{73}$ (conserved in block III, as shown in Figure 1) is located in $\alpha$3 by NMR or in a loop region of the crystal, and its side-chain $H^{\delta}$ (as shown in Figure 5) serves as a proton-donor in the oxyanion hole. Both $Asp^{154}$ and $His^{157}$ (conserved in block V, as shown in Figure 1) are located in a loop region, and they combine with catalytic $Ser^{10}$ to form the catalytic triad.

following the agarose-gel-extraction method. The mutant genes were then subcloned and sequenced in the same manner as the aforementioned wild-type gene.

### Cell growth, protein expression and purification

*E. coli* BL21(DE3) cells transformed with the desired plasmid were grown at 37 °C with 200 rev./min orbital shaking in LB (Luria–Bertani) broth containing 1 % (w/v) Bacto tryptone, 0.5 % (w/v) Bacto yeast extract and 1 % (w/v) NaCl, pH 7.0. For plasmid selection, ampicillin was added to a final concentration of 50 $\mu$g/ml. After the bacteria reached a $D_{600}$ of approx. 0.6, protein overexpression was induced by the addition of IPTG (to a final concentration of 0.4 mM) and cells were incubated at 30 °C for a further 4 h. The cells were harvested by centrifugation (at 17 300 ***g*** for 10 min) and the cell pellet (from 100 ml of LB broth culture) was resuspended in 40 ml of Ni-NTA resin-binding buffer (5 mM imidazole, 0.5 M NaCl and 20 mM Tris/HCl, pH 7.9) and then frozen at − 70 °C for 20 min. After thawing, the suspension was sonicated using an XL-2020 sonicator (Misonix Co.) for 10 pulses of 30 s, with an interval of 30 s, at a setting of approx. 137.5 W, and then centrifuged at 17 300 ***g*** for 20 min at 4 °C. The supernatant containing $His_6$-tagged TAP protein was purified by affinity chromatography using Ni-NTA resin as described previously [10]. The proteins that specifically bound to the column were eluted with 250 mM imidazole. Protein purity was monitored by SDS/PAGE (see below for details), and the protein was dialysed against 25 mM sodium phosphate buffer, pH 7.0.

### SDS/PAGE, Coomassie Brilliant Blue staining and esterase-activity stain of wild-type TAP and mutants

Proteins were analysed by SDS/PAGE [15 % (w/v) gels and 1 % (w/v) SDS]. Protein samples were prepared by the addition of an equal volume of SDS/PAGE loading dye [2 % (w/v) SDS, 200 mM dithiothreitol and 100 mM Tris/HCl, pH 6.8], boiled for 5 min, and then held on ice for 10 min before loading. Each sample was subjected to SDS/PAGE on two separate gels: one was stained with Coomassie Brilliant Blue to analyse protein purity and the other was used for esterase-activity staining, as described previously [23]. Before activity staining, the SDS in the gel was removed by washing twice with 25 % (v/v) propan-2-ol for 30 min each. The gel was then washed in 0.1 M sodium phosphate buffer, pH 7.0, for a further 30 min [24].

### Enzyme kinetic studies of wild-type TAP and mutants

The purified proteins were used for kinetic studies at 37 °C, and all the enzyme activities were determined using spectrophotometry. For simple ester substrate analysis, five concentrations (0.5, 1.0, 1.5, 2.0 and 2.5 mM) of NPB were prepared in 50 mM sodium phosphate buffer, pH 7.0, containing 2.1 % (v/v) Triton X-100. The increase in $A_{405}$ was recorded for 10 min, which was then converted into the production of *p*-nitrophenol per min for initial rate determination [8]. The molar absorption coefficient of *p*-nitrophenol was calculated ($\varepsilon_{405} = 1725\ M^{-1} \cdot cm^{-1}$). For the thioesterase activity assay, six concentrations (25, 50, 75, 100, 150 and 200 mM) of $C_{12}$-CoA were prepared in 0.1 mM DTNB [5,5′-dithiobis-(2-nitrobenzoic acid)], 80 $\mu$g/ml BSA and 50 mM potassium phosphate buffer,

**Table 1 Synthetic oligonucleotides used in site-directed mutagenesis**

The mutated codons are marked in bold, and only the sense primers are shown. As the S10A mutant is too close to the N-terminus of the TAP protein, an NdeI restriction site (underlined) was inserted on the 5′-end to allow subcloning.

| Oligonucleotide sequence 5′ → 3′ | Restriction site | Mutant |
|---|---|---|
| GAT ATA CAT ATG GCG GAC ACG TTA TTG ATT CTG GGT GAT **GCG** CTG AGC | NdeI | S10A |
| AAG CCA CAA TGG ATG CAG GAT **GCG** GGT ATT | | D154A |
| GAC GGT ATT **GCG** CCC AAC CGC | | H157A |
| AAT GCC AGC ATC AGC **GCG** GAC ACC TCG CAA | | G44A |
| GAA CTG GGC GGC **GCG** GAC GGT TTG CGT GGT | | N73A |

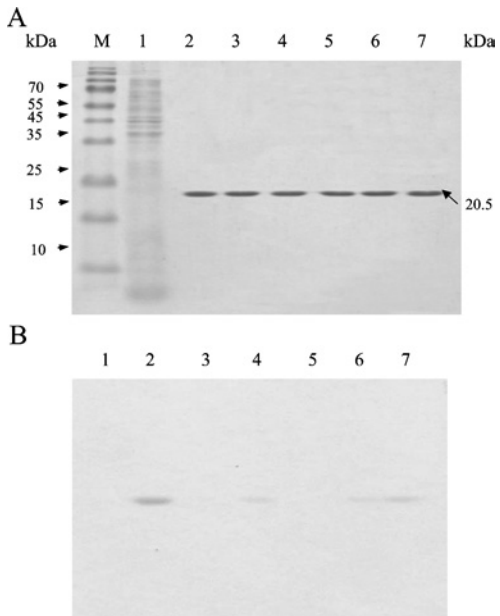


**Figure 3 SDS/PAGE analysis of native and mutant enzymes using protein and activity staining**

Each protein (mutant and wild-type) was purified by affinity chromatography using Ni-NTA resin and was subjected to SDS/PAGE (15% gels, 1% SDS), with 2 $\mu$g of protein loaded into each well. (**A**) Coomassie Brilliant Blue-stained gel. (**B**) Esterase-activity staining (the assay was performed as described in the Experimental section). Lane M, molecular-mass markers (sizes given in kDa); lane 1, the crude extract of the host *E. coli* BL21(DE3) containing plasmid vector pET 20b(+) without *TAP* gene insertion; lane 2, wild-type TAP enzyme; lane 3, mutant S10A; lane 4, mutant D154A; lane 5, mutant H157A; lane 6, mutant G44A; lane 7, mutant N73A.

pH 7.0 [11]. The activity was monitored for 2–6 min and the molar absorption coefficient was calculated ($\varepsilon_{412} = 13\,600\ M^{-1} \cdot cm^{-1}$). For the amino-acid-derived substrate, 2 mM L-NBTNPE was dissolved in 1 ml of dioxane, which was subsequently diluted with 0.1 M sodium phosphate buffer, pH 7.5, to the desired concentrations (25, 50, 75, 100, 150 and 200 mM); the molar absorption coefficient was calculated ($\varepsilon_{400} = 3454\ M^{-1} \cdot cm^{-1}$) [17]. The values of $K_m$ and $k_{cat}$ (kinetic parameters) and means $\pm$ S.D. were calculated from three independent experiments by non-linear regression and were plotted using the Michaelis–Menten equation.

## RESULTS AND DISCUSSION

### Generation and purification of wild-type TAP and mutant enzymes

After subcloning, the mutations in the *TAP* gene were verified by DNA sequencing. The genes were overexpressed in *E. coli* BL21(DE3) cells, and the products were purified to homogeneity, which was shown by Coomassie Brilliant Blue staining of SDS/PAGE gels (Figure 3A). The activity staining of mutants S10A and H157A clearly showed that they had lost hydrolysis activity in response to the substrate $\alpha$-naphthyl butyrate (Figure 3B). Nevertheless, G44A, N73A and D154A retained weak activity in response to the substrate, of which, N73A had the highest residual activity that was consistent with the results of the kinetic studies (Table 2).

### Role of the residues of the catalytic triad and their catalytic parameters

According to the crystallographic structure of the TAP protein, the residues that consist of the catalytic triad, $Ser^{10}$-$His^{157}$-$Asp^{154}$, are lined up in a row on one side of the active-site cleft, with $Ser^{10}$ taking the innermost position in the cleft, and $Asp^{154}$ found nearest the surface of the protein (Figure 2). Figure 4 shows that the distance between $O^{\gamma}$ of $Ser^{10}$ and $N^{\varepsilon 2}$ of $His^{157}$ is 3.02 Å, and $O^{\delta 2}$ and $O^{\delta 1}$ of $Asp^{154}$ are close to $N^{\delta 1}$ and the amide-N of $His^{157}$ with distances of 2.78 and 2.98 Å respectively. When the histidine $N^{\varepsilon 2}$ of the imidazole ring is deprotonated, the three residues in the catalytic triad can co-ordinate each other by hydrogen-bonding, $(Ser^{10})O^{\gamma}$-H $\cdots$ $N^{\varepsilon 2}(His^{157})N^{\delta 1}$-H $\cdots$ $O^{\delta 2}$=C($Asp^{154}$). Hydrogen-bonding between the amide-N of $His^{157}$ and the $O^{\delta 1}$ of $Asp^{154}$ could also presumably strengthen the co-ordination (Figure 4).

In the esterase-activity assay, the $k_{cat}/K_m$ of mutants S10A, D154A and H157A were reduced to 0.57, 18 and 0.09%

**Table 2 Kinetic analysis of wild-type and mutants of TAP**

The kinetic parameters were calculated using the Michaelis–Menten equation with non-linear regression by using NPB, $C_{12}$-CoA and L-NBTNPE as substrates at 37°C, pH 7. Data are means $\pm$ S.D. for three independent experiments. The data in the parentheses show the relative values to those of the wild type. ND, not determined.

| Substrate | Parameter | Wild-type | S10A | D154A | H157A | G44A | N73A |
|---|---|---|---|---|---|---|---|
| NPB | $k_{cat}$ ($s^{-1}$) | 15.29 $\pm$ 0.79 | 0.16 $\pm$ 0.01 (1.0%) | 5.98 $\pm$ 0.59 (39%) | 0.0093 $\pm$ 0.0007 (0.06%) | 3.16 $\pm$ 0.08 (21%) | 11.99 $\pm$ 2.13 (78%) |
| | $K_m$ (mM) | 0.87 $\pm$ 0.13 | 1.55 $\pm$ 0.18 (1.78-fold) | 1.88 $\pm$ 0.37 (2.16-fold) | 0.61 $\pm$ 0.18 (0.70-fold) | 1.10 $\pm$ 0.14 (1.26-fold) | 1.66 $\pm$ 0.35 (1.91-fold) |
| | $k_{cat}/K_m$ | 17.75 (100%) | 0.10 (0.57%) | 3.18 (18%) | 0.015 (0.09%) | 2.87 (16%) | 7.22 (41%) |
| $C_{12}$-CoA | $k_{cat}$ ($s^{-1}$) | 10.13 $\pm$ 0.87 | 0.057 $\pm$ 0.007 (0.6%) | 0.45 $\pm$ 0.01 (4%) | ND | 0.77 $\pm$ 0.04 (7.6%) | 1.14 $\pm$ 0.08 (11.3%) |
| | $K_m$ (mM) | 0.146 $\pm$ 0.022 | 0.127 $\pm$ 0.028 (0.87-fold) | 0.059 $\pm$ 0.005 (0.40-fold) | ND | 0.075 $\pm$ 0.008 (0.51-fold) | 0.085 $\pm$ 0.016 (0.58-fold) |
| | $k_{cat}/K_m$ | 69.44 (100%) | 0.45 (0.6%) | 7.62 (11%) | ND | 10.19 (15%) | 13.35 (19%) |
| L-NBTNPE | $k_{cat}$ ($s^{-1}$) | 88.99 $\pm$ 3.97 | 0.02 $\pm$ 0.00 (0.02%) | 6.44 $\pm$ 0.28 (7.2%) | ND | 7.71 $\pm$ 0.21 (8.7%) | 7.81 $\pm$ 0.09 (8.8%) |
| | $K_m$ (mM) | 0.174 $\pm$ 0.014 | 0.061 $\pm$ 0.010 (0.35-fold) | 0.043 $\pm$ 0.007 (0.25-fold) | ND | 0.060 $\pm$ 0.005 (0.34-fold) | 0.044 $\pm$ 0.002 (0.25-fold) |
| | $k_{cat}/K_m$ | 512.40 (100%) | 0.32 (0.06%) | 149.64 (29%) | ND | 127.94 (25%) | 178.86 (35%) |

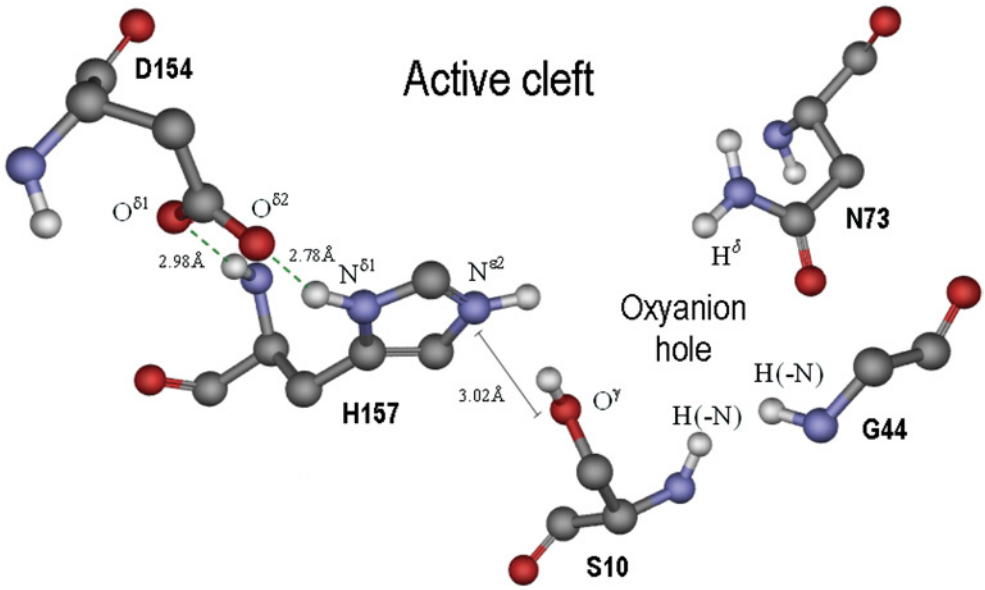


**Figure 4 The active cleft of TAP solved by crystallography [21]**

The left-hand side is lined with three catalytic triad residues, Asp[154], His[157] and Ser[10]. When active Ser[10] attacks the ester substrate, an oxyanion intermediate will form, which will be stabilized with the residues on the right-hand side, Gly[44] and Asn[73]. Each atom of the amino acid residues that is involved in the interaction with substrate or with the other residues in the diagram is denoted using amino acid side-chain nomenclature. $N^{\varepsilon2}$ of His[157] in the imidazole ring is protonated in the Figure, but the catalytic activity can only be performed when the proton is dissociated, by which the lone electron pair of $N^{\varepsilon2}$-His[157] is provided for the attraction of $H^{\gamma}$-Ser[10]. The Figure was prepared using the ViewerLite (version 5.0) program.

respectively. Mutant H157A showed very low activity, which was measured by the addition of a large amount of enzyme, combined with a prolonged reaction time. Therefore this mutant was omitted for the other two enzymatic assays. His[157] obviously plays the most important role in the catalytic triad by acting as a connector between Ser[10] and Asp[154]. For mutants S10A and D154A, all three substrates were used to monitor their catalytic parameters.

### S10A

For direct targeting of the catalytic serine residue, Ser[10], the crystal structure of TAP enzyme covalently bound to the serine-enzyme inhibitor DEP (diethyl *p*-nitrophenyl phosphate) was solved (PDB code 1J00) (Figure 5) [25]. The covalent bond between Ser[10] $O^{\gamma}$ and the phosphorus of the DEP molecule indicated that Ser[10] is devoted to nucleophilic attack on the carbonyl-C of an ester bond in a regular catalysis reaction. The $N^{\varepsilon2}$ of His[157] formed hydrogen bonds with the phosphorus oxygen of DEP and no longer interacted with the catalytic Ser[10]. The corresponding positions of His[157] and Asp[154] remained in the same conformation as the wild-type TAP structure (Figure 4). When NPB was used as the enzyme substrate, the mutant S10A gave a $K_m$ value that was approx. 2-fold greater than that of the wild-type and a $k_{cat}$ value that was only 1.0 % of the wild-type (Table 2). When $C_{12}$-CoA was used as the substrate, the mutant retained 0.6 % of the $k_{cat}$ value (compared with the wild-type) and had a similar $K_m$ value. The weak activity of S10A suggests that a water molecule in the active centre [26] could replace the hydroxy group of Ser[10] to attack the carbonyl-C of ester, and that the water molecule could be activated by His[157], which serves as proton acceptor, although through a much slower catalytic mechanism. When catalysing L-NBTNPE, S10A acted even more weakly, with only 0.02 % of the $k_{cat}$ activity compared with the wild-type. However, the $K_m$ value was reduced to approx. one-third of the wild-type. The lower $K_m$ perhaps indicates that the higher hydrophobic active centre of S10A is more accessible to L-NBTNPE, a more hydrophobic substrate. It could also be assumed that L-NBTNPE may interfere in the proper positioning of a water molecule in the formation of the hydroxy-L-NBTNPE tetrahedral intermediate.

### D154A

In the three enzymatic assays, D154A retained 18, 11 and 29 % of its catalytic efficiency compared with the wild-type in response to the substrates NPB, $C_{12}$-CoA and L-NBTNPE respectively, which suggests that Asp[154] is not essential for catalysis. Asp[154] is positioned close to the entrance of the substrate tunnel on the protein surface (Figure 2), therefore it could significantly affect enzymatic activity by altering substrate accessibility. Of the three substrates, NPB is the most hydrophilic and, as a result, had an increased $K_m$ value of $1.88 \pm 0.37$ mM (an approx. 2-fold increase compared with the wild-type). However, decreased $K_m$ values were observed for the substrates $C_{12}$-CoA and L-NBTNPE (40 and 25 % of the wild-type respectively), which are themselves hydrophobic compounds. These observations are consistent with the expected effect of replacing an aspartic acid residue with the more hydrophobic alanine residue. Therefore the reduced catalytic efficiency was a result of significantly lower $k_{cat}$ values. In response to NPB, the mutant retained 39 % of the $k_{cat}$ value compared with the wild-type. In addition to the hydrophobic effect, molecular size is an important distinction between the three substrates. The difference between the reduced $k_{cat}$ values for $C_{12}$-CoA and L-NBTNPE (4 and 7.2 % compared with the wild-type respectively) and the less-affected $k_{cat}$ value for NPB could, in part, result from the larger size of the $C_{12}$-CoA and L-NBTNPE substrates compared with NPB. $O^{\delta2}$-Asp[154] attracts the proton of $N^{\delta1}$-His[157] (Figure 4), which could draw His[157] backwards to provide a larger space during substrate binding. The methyl side-chain of D154A is presumed to not only weaken the hydrogen-bonding link between the residues of the catalytic triad, but also to diminish the His[157] spanning area, which is consistent with

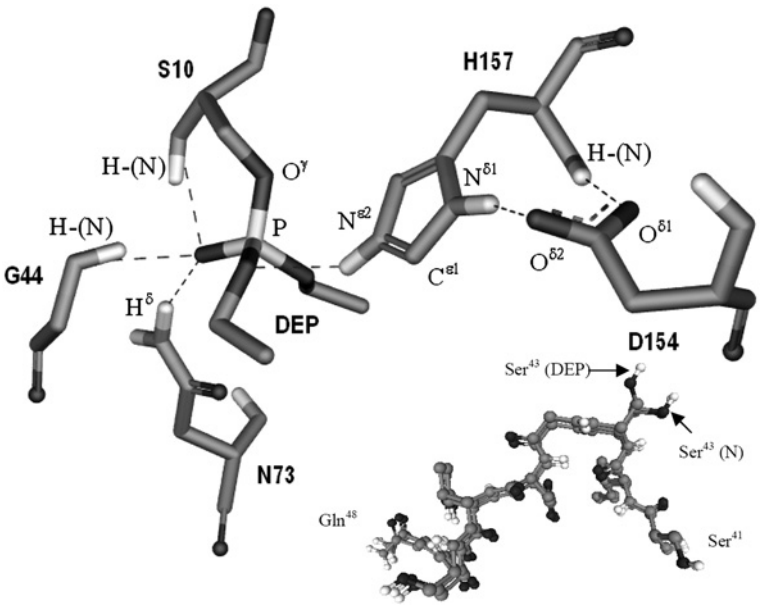


**Figure 5 Active centre of DEP–TAP complex structure**

The crystallographic structure (PDB code 1J00) [22] shows DEP covalently bound to Ser$^{10}$, which indicates that Ser$^{10}$ is acting as a nucleophilic attacker towards the ester bond of substrate. The broken lines denote possible hydrogen-bonding between atoms. Amide protons of Ser$^{10}$ and Gly$^{44}$ could serve as hydrogen-bond donors for oxyanion. H$^{\delta}$ of Asn$^{73}$ could devote further constraint by hydrogen-bonding to stabilizing oxyanion structure. After activating Ser$^{10}$, the HN$^{\varepsilon2}$ of His$^{157}$ may serve as a hydrogen-bond donor for the bound substrate in the transition state. The inset shows the superimposition of the region S$^{41}$ISGDTSQ$^{48}$ of the two structures, native TAP (PDB code 1IVN, denoted by N) and TAP–DEP complex (PDB code 1J00, denoted by DEP). Ser$^{43}$ extends its side chain in a distinctly different direction in the two situations. The Figure was prepared using the ViewerLite (version 5.0) program.

the observed decline in $k_{cat}$ values in response to the two larger substrates, $C_{12}$-CoA and L-NBTNPE.

### H157A

For NPB substrate, H157A had similar $K_m$ value ($0.61 \pm 0.18$ mM) compared with the wild-type ($0.87 \pm 0.13$ mM); however, it had a dramatically reduced $k_{cat}/K_m$ value (0.09 % of the wild-type). This indicates that, without the hydrogen-bonding between the side chains of His$^{157}$ and Ser$^{10}$, the ester substrate retains approximate accessibility to the active cleft, and thus the barely detectable catalytic efficiency resulted from the extremely low $k_{cat}$ value ($0.0093 \pm 0.0007$ s$^{-1}$) of the mutant. H157A had only 5.8 % of the $k_{cat}$ activity of the S10A mutant, which supposedly performed catalysis aided by a water molecule in the active cleft. The crystal data of the TAP–DEP complex showed that the N$^{\varepsilon2}$ of His$^{157}$ interplayed with the inhibitor DEP (Figure 5) therefore His$^{157}$ could probably stabilize the acyl–enzyme intermediate during the catalytic process. We conclude that His$^{157}$ is the most important residue in the catalytic triad, as it is responsible for the activation of the catalytic serine, and also for its contribution to the hydrogen-bonding of the acyl–enzyme intermediate in the catalysis machinery.

## Mutation of the residues involved in the oxyanion hole

Oxyanion is formed when Ser$^{10}$-O$^{\gamma}$H attacks ester carbonyl-C, whose covalent $\pi$ electron pair shifts on to the carbonyl-O. The oxyanion is so unstable that the DEP molecule covalently bound to TAP mimics the untraceable enzyme–substrate-intermediate [25]. The NMR data showed that a large chemical-shift perturbation was observed upon conversion from the TAP–DEP Michaelis complex into the tetrahedral complex. The amide protons of Ser$^{10}$ and Gly$^{44}$ act as proton donors in the oxyanion hole, which stabilize the tetrahedral adduct. X-ray crystallography of TAP–DEP identified that Asn$^{73}$ offers its H$^{\delta}$ for hydrogen-bonding to the oxyanion [25] (Figure 5). The mutants G44A and N73A were analysed using the same substrates as the kinetic study.

### G44A

In response to NPB, G44A retained a $k_{cat}$ value that was 21 % of the wild-type enzyme and had little change in the $K_m$ value. The significant reduction in the $k_{cat}$ activity ($3.16 \pm 0.08$ s$^{-1}$ compared with $15.29 \pm 0.79$ s$^{-1}$ for the wild-type) was caused by the methyl group of the alanine residue replacing the H$^{\alpha}$ of Gly$^{44}$, which indicates that the heavier side chain disturbed tetrahedral-intermediate formation, but had little effect on accessibility of the substrate. For substrates $C_{12}$-CoA and L-NBTNPE, the decreased $K_m$ values gave further assurance that replacing the target residue with alanine did not handicap the substrate binding. The reduced catalytic efficiency in response to $C_{12}$-CoA and L-NBTNPE was predominantly caused by the reduced $k_{cat}$ activity (only 7.6 and 8.7 % compared with the wild-type activity respectively).

The crystal structure comparison of both native TAP and TAP–DEP complex revealed no difference in the position of Gly$^{44}$ (shown in Figure 5, inset). They could actually be superimposed using Gly$^{44}$ and the nearby residues, with the exception of the unique side chain of Ser$^{43}$ (Figure 5 inset). The angles, $\phi$ and $\psi$, of Ser$^{43}$ in the TAP and the TAP–DEP structures are: $\phi$ $-64.47°$ and $\psi$ 140.07°, and $\phi$ $-54.41°$ and $\psi$ 134.47° respectively. However, the side chain of Ser$^{43}$ is too distant to form any hydrogen-bonding with the DEP molecule in TAP–DEP structure.

It is proposed that the conversion from the TAP–DEP Michaelis complex into the tetrahedral complex involves Gly$^{44}$ movement, and that the movement of Gly$^{44}$ also draws on the movements of the neighbouring residues. Glycine has the most freely rotatable C$^{\alpha}$ $\phi$ and $\psi$ angles among the 20 amino acid residues in the protein folding structure, and that is due to the presence of the smallest side chain, hydrogen. The significant alteration of

the Ser[43] side chain position and the highly decreased $k_{cat}$ of G44A (in response to all three substrates) suggests that the less restrained movement of Gly[44] is important in conformational fine-tuning during oxyanion formation.

N73A

N73A retained 78 % of $k_{cat}$ activity and had a $K_m$ that was approx. 2-fold greater compared with the wild-type TAP in response to NPB. Nevertheless, its $k_{cat}$ activity was reduced to approx. one-tenth of the wild-type activity in response to $C_{12}$-CoA and L-NBTNPE (11.3 and 8.8 % respectively), and also had decreased $K_m$ values (0.58- and 0.25-fold compared with the wild-type respectively). The hydrophilic amide side chain of Asn[73] obviously had decreased accessibility for hydrophobic substrates ($C_{12}$-CoA and L-NBTNPE), because lower $K_m$ values were observed when this residue was replaced with an alanine residue. In contrast, the smallest and most hydrophilic substrate, NPB, increased its $K_m$ value 1.91-fold in response to the N73A mutation.

In SGNH-hydrolases, the oxyanion hole has three hydrogen-bond donors. In TAP, the three proton donors are Ser[10] and Gly[44] with amide protons, and Asn[73] with $H^{\delta}$ (Figure 5). No striking decline in the catalytic efficiency of the N73A mutant compared with the wild-type was observed. As Asn[73] is considered to provide one-third of the hydrogen-bonding contribution to the stabilization of the oxyanion, thus the lower activity of the N73A mutant is proposed to be due to the remaining two-thirds of the hydrogen-bonding from the Ser[10] and Gly[44] residues. The lowest activity in response to $C_{12}$-CoA (19 %), a long fatty-acyl substrate, indicates that fatty-acyl substrate is predominantly affected compared with the other two substrates. Asn[73] is close to the switch $loop_{75-80}$ that was recently reported to show a remarkable conformational change in the crystal structure of TAP-OCA (native TAP soaked with octanoic acid; PDB code 1U8U) [27], which indicated that Asn[73] was capable of accommodating longer acyl-chain-length substrates. Although the position of Asn[73] in both the TAP and TAP-OCA structures is consistent, the function for longer-acyl substrate accommodation by $loop_{75-80}$ is considered to be correlated with the Asn[73] residue. We propose that the role of Asn[73] is also involved in the $loop_{75-80}$ switch-move motion, and is therefore more essential for accommodation of longer acyl-chain-length substrates.

## Conclusions

The catalytic triad Ser[10]-Asp[154]-His[157], as well as the oxyanion-stabilizing residues Gly[44] and Asn[73], of the TAP enzyme were mutated to evaluate their roles in catalytic behaviour. Of the residues, His[157] is the most important as it plays a vital role in the catalytic triad, and may also be devoted to stabilizing the oxyanion-intermediate conformation. Ser[10] is a very important residue in the mechanism and a water molecule can, at best, act as a poor replacement. The water molecule could possibly possess the nucleophilic-attacking character that is endowed by His[157] hydrogen-bonding. Asp[154] is not essential compared with the other residues in the catalytic triad. It is located close to the entrance of the substrate tunnel, therefore it predominantly affects substrate accessibility. The effect of Asp[154] withdrawal of His[157] is proposed to provide a larger active cleft, which would allow the accommodation of bigger substrates. Gly[44] plays a role in the stabilization of the oxyanion intermediate. The side-chain position of Ser[43] in TAP–DEP differed from that of the native TAP, and the reduced $k_{cat}$ values observed for the G44A mutant in response to the three substrates suggests that Gly[44] is also involved in accommodating the acyl-enzyme-intermediate transformation. N73A showed the highest residual enzyme activity among all of the mutants, which indicates that Asn[73] is not as essential in the catalytic process as the other mutated residues.

We are grateful to Dr K. C. Tsai in the Genomics Research Centre, Academia Sinica, Taiwan, for plot production. We thank the computer modelling training course provided by National Centre for High-Performance Computing, Hsinchu Science Park, Hsinchu 30076, Taiwan. This work was supported by a grant [National Science and Technology Programme for Agricultural Biotechnology (23-71)] to J.-F. S., and a grant (NSC 92-2311-B-030-002) to Y.-L. L. from the National Science Council, Republic of China.

## REFERENCES

1 Klibanov, A. M. (1990) Asymmetric transformations catalyzed by enzymes in organic solvents. Acc. Chem. Res. **23**, 114–120
2 Gandhi, N. N. (1997) Applications of lipase. J. Am. Oil Chem. Soc. **74**, 621–634
3 Upton, C. and Buckley, J. T. (1995) A new family of lipolytic enzymes? Trends Biochem. Sci. **20**, 178–179
4 Molgaard, A., Kauppinen, S. and Larsen, S. (2000) Rhamnogalacturonan acetylesterase elucidates the structure and function of a new family of hydrolases. Structure **8**, 373–383
5 Li, J., Derewenda, U., Dauter, Z., Smith, S. and Derewenda, Z. S. (2000) Crystal structure of the *Escherichia coli* thioesterase II, a homolog of the human Nef binding enzyme. Nat. Struct. Biol. **7**, 555–559
6 Akoh, C. C., Lee, G. C., Liaw, Y. C., Huang, T. H. and Shaw, J. F. (2004) GDSL family of serine esterases/lipases. Prog. Lipid Res. **43**, 534–552
7 Shaw, J. F., Chang, R. C., Chuang, K. H., Yen, Y. T., Wang, Y. J. and Wang, F. G. (1994) Nucleotide sequence of a novel arylesterase gene from *Vibro mimicus* and characterization of the enzyme expressed in *Escherichia coli*. Biochem. J. **298**, 675–680
8 Chang, R. C., Chen, J. C. and Shaw, J. F. (1996) Site-directed mutagenesis of arylesterase from *Vibrio mimicus* identifies residues essential for catalysis. Biochem. Biophys. Res. Commun. **221**, 477–483
9 Lee, Y. L., Chen, J. C. and Shaw, J. F. (1997) The thioesterase of *Escherichia coli* has arylesterase activity and shows stereospecificity for protease substrates. Biochem. Biophys. Res. Commun. **231**, 452–456
10 Lee, Y. L., Su, M. S., Huang, T. H. and Shaw, J. F. (1999) C-terminal His-tagging results in substrate specificity changes of the thioesterase I from *Escherichia coli*. J. Am. Oil Chem. Soc. **76**, 1113–1118
11 Cho, H. and Cronan, Jr, J. E. (1993) *Escherichia coli* thioesterase I, molecular cloning and sequencing of the structural gene and identification as a periplasmic enzyme. J. Biol. Chem. **268**, 9238–9245
12 Pacaud, M. and Uriel, J. (1971) Isolation and some properties of a proteolytic enzyme from *Escherichia coli* (protease I). Eur. J. Biochem. **23**, 435–442
13 Albright, F. R., White, D. A. and Lennarz, W. J. (1973) Studies on enzymes involved in the catabolism of phospholipids in *Escherichia coli*. J. Biol. Chem. **248**, 3968–3977
14 Doi, O. and Nojima, S. (1975) Lysophospholipase of *Escherichia coli*. J. Biol. Chem. **250**, 5208–5214
15 Pacaud, M., Sibilli, L. and LeBras, G. (1976) Protease I from *Escherichia coli*. Eur. J. Biochem. **69**, 141–151
16 Karasawa, K., Kudo, I., Kobayashi, T., Homma, H., Chiba, N., Mizushima, H., Inove, K. and Nojima, S. (1991) Lysophospholipase L1 from *Escherichia coli* K-12 overproducer. J. Biochem. **109**, 288–293
17 Ichihara, S., Matsubara, Y., Kato, C., Akasaka, K. and Mizushima, S. (1993) Molecular cloning, sequencing, and mapping of the gene encoding protease I and characterization of proteinase and proteinase-defective *Escherichia coli* mutants. J. Bacteriol. **175**, 1032–1037
18 Cho, H. and Cronan, Jr, J. E. (1994) 'Protease I' of *Escherichia coli* functions as a thioesterase *in vivo*. J. Bacteriol. **176**, 1793–1795
19 Lin, T. H., Chen, C., Haung, R. F., Lee, Y. L., Shaw, J. F. and Huang, T. H. (1998) Multinuclear NMR resonance assignments and the secondary structure of *Escherichia coli* thioesterase/protease I: a member of a new subclass of lipolytic enzymes. J. Biomol. NMR **11**, 363–380
20 Huang, Y. T., Liaw, Y. C., Gorbatyuk, V. Y. and Huang, T. H. (2001) Backbone dynamics of *Escherichia coli* thioesterase/protease I: evidence of a flexible active-site environment for a serine protease. J. Mol. Biol. **307**, 1075–1090
21 Lo, Y. C., Lee, Y. L., Shaw, J. F. and Liaw, Y. C. (2000) Crystallization and preliminary X-ray crystallographic analysis of thioesterase I from *Escherichia coli*. Acta Crystallogr. Sect. D: Biol. Crystallogr. **56**, 756–757

22 Lo, Y. C., Lin, S. C., Shaw, J. F. and Liaw, Y. C. (2003) Crystal structure of *Escherichia coli* thioesterase I/protease I/lysophospholipase L1: consensus sequence blocks constitute the catalytic centre of SGNH-hydrolases through a conserved hydrogen bond network. J. Mol. Biol. **330**, 539–551
23 Tanksley, S. D. and Orton, T. T. (1983) Isozymes in Plant Genetics and Breeding, Part A, Elsevier Science Publishers, East Linn
24 Blank, A., Sugiyama, R. H. and Deffer, C. A. (1982) Activity staining of nucleolytic enzymes after sodium dodecyl sulphate-polyacrylamide gel electrophoresis: use of aqueous isopropanol to remove detergent from gels. Anal. Biochem. **120**, 267–275
25 Tyukhtenko, S. I., Litvinchuk, A. V., Chang, C. F., Lo, Y. C., Lee, S. J., Shaw, J. F., Liaw, Y. C. and Huang, T. H. (2003) Sequential structural changes of *Escherichia coli* thioesterase/protease I in the serial formation of Michaelis and tetrahedral complexes with diethyl *p*-nitrophenyl phosphate. Biochemistry **42**, 8289–8297
26 Benning, M. M., Wesenberg, G., Liu, R., Taylor, D. L., Dunaway-Marianos, D. and Holden, H. M. (1998) The three-dimensional structure of 4-hydroxybenzoyl-CoA thioesterase from *Pseudomonas* sp. strain CBS-3. J. Biol. Chem. **273**, 33572–33579
27 Lo, Y. C., Lin, S. C., Shaw, J. F. and Liaw, Y. C. (2005) Substrate specificities of *Escherichia coli* thioesterase I/protease I/lysophospholipase $L_1$ are governed by its switch loop movement. Biochemistry **44**, 1971–1979

Received 10 October 2005/27 February 2006; accepted 6 March 2006
Published as BJ Immediate Publication 6 March 2006, doi:10.1042/BJ20051645